NASA/TM-20230003044

B_4C-Al Metal Matrix Composites for Extreme Space Environments

Sang-Hyon Chu, Cheol Park, and Terryl Wallace
NASA Langley Research Center, Hampton, Virginia

Calista Lum
Department of Physics, School of Natural Sciences, University of California, Merced, California

John Lyons
Department of Chemical Engineering, University of Kentucky, Lexington, Kentucky

Donghyun Lee, Junghwan Kim, Seungchan Cho, and Sang-Bok Lee
Functional Composites Department, Composites Research Division, Korea Institute of Materials Science, Changwon 51508, Republic of Korea

March 2023

NASA STI Program Report Series

The NASA STI Program collects, organizes, provides for archiving, and disseminates NASA's STI. The NASA STI program provides access to the NTRS Registered and its public interface, the NASA Technical Reports Server, thus providing one of the largest collections of aeronautical and space science STI in the world. Results are published in both non-NASA channels and by NASA in the NASA STI Report Series, which includes the following report types:

- TECHNICAL PUBLICATION. Reports of completed research or a major significant phase of research that present the results of NASA Programs and include extensive data or theoretical analysis. Includes compilations of significant scientific and technical data and information deemed to be of continuing reference value. NASA counterpart of peer-reviewed formal professional papers but has less stringent limitations on manuscript length and extent of graphic presentations.

- TECHNICAL MEMORANDUM. Scientific and technical findings that are preliminary or of specialized interest, e.g., quick release reports, working papers, and bibliographies that contain minimal annotation. Does not contain extensive analysis.

- CONTRACTOR REPORT. Scientific and technical findings by NASA-sponsored contractors and grantees.

- CONFERENCE PUBLICATION. Collected papers from scientific and technical conferences, symposia, seminars, or other meetings sponsored or co-sponsored by NASA.

- SPECIAL PUBLICATION. Scientific, technical, or historical information from NASA programs, projects, and missions, often concerned with subjects having substantial public interest.

- TECHNICAL TRANSLATION. English-language translations of foreign scientific and technical material pertinent to NASA's mission.

Specialized services also include organizing and publishing research results, distributing specialized research announcements and feeds, providing information desk and personal search support, and enabling data exchange services.

For more information about the NASA STI program, see the following:

- Access the NASA STI program home page at http://www.sti.nasa.gov

- Help desk contact information:

https://www.sti.nasa.gov/sti-contact-form/ and select the "General" help request type.

NASA/TM-20230003044

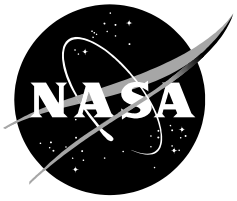

B_4C-Al Metal Matrix Composites for Extreme Space Environments

Sang-Hyon Chu, Cheol Park, and Terryl Wallace
NASA Langley Research Center, Hampton, Virginia

Calista Lum
Department of Physics, School of Natural Sciences, University of California, Merced, California

John Lyons
Department of Chemical Engineering, University of Kentucky, Lexington, Kentucky

Donghyun Lee, Junghwan Kim, Seungchan Cho, and Sang-Bok Lee
Functional Composites Department, Composites Research Division, Korea Institute of Materials Science, Changwon 51508, Republic of Korea

National Aeronautics and
Space Administration

Langley Research Center
Hampton, VA 23681

March 2023

Acknowledgments

The authors would like to express their appreciation to NASA Langley Research Center, Center Innovation Fund (CIF) program under Space Technology Mission Directorate (STMD) for their support. The authors from Korea Institute of Materials Science (KIMS) were supported by the National Research Foundation of Korea (NRF) grant funded by the Korea government (MSIP) (2022M3H4A3046292).

Available from:

NASA STI Program / Mail Stop 148
NASA Langley Research Center
Hampton, VA 23681-2199
Fax: 757-864-6500

Abstract

Extreme space environments such as space vacuum, radiation, thermal extremes and cycles, jagged lunar dust, microgravity, micrometeoroids and orbit debris (MMOD), thrust plume ejecta, and their synergistically-adverse effects are difficult challenges for safe and sustainable space exploration to outer planets and satellites. Prolonged space radiation exposure embrittles materials and structures and abrasive jagged dust particles aggressively wear and erode moving parts leading to premature failure. To counter or even alleviate such potential failures, robust and exceptional materials are needed to make NASA missions including Artemis program sustainable with minimum service and repair needs. This study reports that boron-containing inclusion, B_4C, can improve wear resistance and radiation shielding/resistance of aluminum alloy (Al6061) significantly to extend the service life in extreme space environments. With increasing B_4C inclusions, the tensile strength increased up to 20 vol% at both room temperature and an elevated temperature (200˚C) while thermal conductivity decreased gradually as a function of B_4C concentration. The neutron shielding effectiveness increased more than 110 times when 50 vol% B_4C is incorporated in Al6061 when compared with the pristine Al6061. The shielding effectiveness under galactic cosmic rays (GCR) and solar particle events (SPE) was also studied computationally using on-line tool for the assessment of radiation in space (OLTARIS). By adding B_4C, the adverse effect caused by secondary radiation through the Al6061 matrix was effectively suppressed to improve the shielding effectiveness against GCR and SPE. The presence of boron in B_4C was the main reason for the enhanced radiation shielding capability against neutron, GCR, and SPE environments.

1. Introduction

NASA has pursued human space exploration programs and deep-space flight missions while broadening collaboration with U.S. commercial space industry and international partners in the Artemis program and Commercial Lunar Payload Services (CLPS) [1-3]. During the space missions, astronauts, space vehicles, and scientific instruments are subject to extreme space environments including space vacuum, microgravity, thermal cycles, space radiation, abrasive lunar dust, and micrometeorite and orbital debris (MMOD). The impacts of the extreme space environment become more severe in the case of the crewed, prolonged space missions.

Space radiation is considered as one of the most challenging risks for the human space exploration beyond Low Earth Orbit (LEO). Unlike radiations of high energy photons and energetic beta particles emitted from the radioisotope power sources while undergoing transmutation process, space radiation includes geomagnetically trapped energetic charged particles in the Van Allen belts, galactic cosmic rays (GCR), solar particle events (SPE), and secondary albedo radiation. The electrons and protons trapped in the Earth's magnetic field have low energy enough that a typical mass shielding of space systems can provide significant protection. However, the trapped particles can still cause degradation of microelectronics, solar cells, and optical components [4,5]. GCR are the most energetic particles stripped of all electrons during interstellar travel at close to the speed of light, consisting of protons (85%), alpha particles or helium nuclei (14%), and high-charge high-energy (HZE) particles (1%) [4,6]. From the viewpoint of relative biological effectiveness (RBE), HZE particles and neutron-generated nuclear recoils can cause nearly 20 times higher RBE than protons, implying severe damage to living tissues. While GCR are always present, SPE are unpredictable and lasting for several days. SPE generate high energy protons and heavy ions in coronal mass ejections (CME) followed by solar flares. In comparison with GCR protons, SPE protons can carry energies up to tens of GeV, causing major single event effects (SEE), ionizing dose, and displacement damage [5,6].

Such GCR and SPE particles interact with the planetary atmosphere and soil, producing a cascade of secondary particles such as abundant neutrons on the Lunar and Martian surface [7-9]. In the case of massive space structures like the International Space Station (ISS), the secondary neutrons are the main radiation source caused by energetic interaction of incoming space radiation with Aluminum in their shell walls [9,10]. The presence of significant secondary neutrons can be potential threats to the safety of the crews and the success of space missions because high linear energy transfer (LET) of neutrons imposes significant damage to biological cells and sophisticated microelectronics at their paths [11]. Neutron has a mass of 1.67×10^{-27} kg that is similar to that of proton and is electrically neutral. Therefore, hydrogen-rich polymers like polyethylene or boron-containing composites are considered to be effective for slowing down neutrons under elastic collision without generating heavy particle fragments [12]. Boron-containing reinforcements are added to neutron shielding materials because of boron's excellent capability of neutron absorption. Especially, ^{10}B, a stable isotope of the naturally occurring boron has a high neutron capture cross section (3840 barns, at 300 K) for low-energy thermal neutrons [13].

B_4C-Al metal matrix composites (MMC) have gained a broad attention because of their lightweight, high strength, wear resistance, and excellent thermal stability. In this study, B_4C was used as a boron-containing neutron absorber and incorporated into aerospace-grade Al6061 alloy to produce B_4C-Al MMC with up to 50 vol.% B_4C. The neutron shielding effectiveness was experimentally evaluated with a neutron source and then theoretically studied using computational modeling tools for space radiation environments in GCR and SPE radiations. Based on the current results, we report that B_4C-Al MMC might be a potential candidate for load-bearing structural materials in on-orbit and on-ground space structures in extreme space environments.

2. Experimental

2.1. Fabrication of B_4C-Al MMC

B_4C powders (Dunhua Zhengxing Abrasive, China) of commercial grade F320 with the average size of 39.0 ± 1.5 μm and Al6061 alloy (ThyssenKrupp Materials Korea, Republic of Korea) were used as raw materials. A combined process of stir casting and hot rolling was used to effectively produce 0, 5, 10, and 20 vol.% B_4C-reinforced Al MMC in this research. Using an induction heating system, the Al6061 alloy was melted at 750°C in a graphite mold. Using a custom-designed two-bladed impeller, molten Al alloy was stirred at 800 rpm strenuously to form a vortex at the surface of the melt and the detailed process was reported previously [14]. Then, 5, 10, and 20 vol.% B_4C powder was introduced into the molten Al alloy using a powder input nozzle, respectively. The stirring was continued for about 10 min before the slurry was cast. For the hot rolling process, the cast B_4C-Al MMC with a thickness of 10 mm were annealed first at the rolling temperature at 400˚C for 1 hr. The rolling pass was conducted to fabricate B_4C-Al composite sheets. The rolling reduction was about 5% during each rolling pass. Each MMC sample was annealed at the rolling temperature at 400˚C for 5 min during each rolling cycle. The schematic of the stir casting and hot rolling processes is shown in the top image of Figure 1. On the other hand, for the Al MMC with high B_4C concentrations, a liquid pressing process was employed to produce 30 vol.% and 50 vol.% B_4C-Al MMC samples. A B_4C powder layer and an Al6061 plate were placed into a steel mold (inner dimensions: 100 mm × 100 mm × 10 mm), as illustrated in the bottom image of Figure 1. The mold was heated to 700°C, held for 5 min, and then hydrostatically pressed at about 10 MPa. During the liquid pressing process, the molten Al plate was infiltrated into the B_4C powder layer. The pristine Al6061 control and B_4C-Al MMC samples with a diameter of 25.4 mm and a thickness of around 2 mm are shown in Figure 2. The morphological characteristics of the fabricated B_4C-Al MMC samples were investigated using a scanning electron microscope (SEM; JSM-6610LV, JEOL, Japan). Tensile properties were measured with a tensile tester (5882 model, INSTRON, USA) at room temperature and an elevated temperature 200˚C. Flat tensile specimens of the dimensions in accordance with sub-sized ASTM E8/E8M-11 standards were used to conduct the tests and the strain rate was 5×10^{-4} s^{-1}. Hardness was determined with a microhardness tester (Buehler Micromet 5103) using a Vickers hardness indenter with 500 gf and 10 sec dwelling time. Thermal conductivity was assessed using a laser flash analyzer (Netzsch 467, NETZSCH, Germany) through the thickness by measuring the thermal diffusivity along with heat capacity.

2.2. Neutron shielding experiment

Neutron shielding measurements on the B_4C-Al MMCs were made using a neutron activation analysis. For a neutron shielding test, a circular piece of pure indium (In) foil with a diameter of 25 mm and a thickness of around 1.0 mm was covered with the material to be studied as a shielding material. The In foil (AA) was exposed to a one-Curie Americium (^{241}Am)-Beryllium (^{9}Be) neutron source (4.5 MeV) through the shielding material in the test, as illustrated in Figure 3. The neutron source encapsulated in stainless steel was safely placed inside a hole drilled at the center of a stack of 2.54 cm-thick phenolic plates surrounded by lead bricks. To moderate the neutron emission, a polyethylene (PE) block was placed in front of the Am-Be neutron source. The set of In foil and test material was placed to the PE block and exposed to the neutron irradiation at a dose rate of 300 mrem/hr so that the ^{115}In could be activated to ^{116}In by neutrons. The neutron exposure was conducted overnight for the activation equilibrium. In the next day, the activated In foil was removed from the test sample and counted using a Geiger-Mueller (GM) probe with a digital counter (SpecTech ST360, TN). The first activity count started one minute after the removal of the activated In foil from the neutron source, followed by the collection of counts for 100 seconds at two-minute intervals for total two hours. Since the activated ^{116}In decays with a half-life of 54 minutes, the counting can be completed in two hours or two half-lives. When the neutron shielding effectiveness of the material increases, the radioactivity induced in the In foil decreases because of the neutron capture by the shielding material. The neutron shielding test via the In

activation was conducted for a pristine Al6061 control and B_4C-Al MMC materials, respectively. The activation at saturation or GM probe count at time t = 0 was determined for each material by extrapolation of the count plot to t = 0.

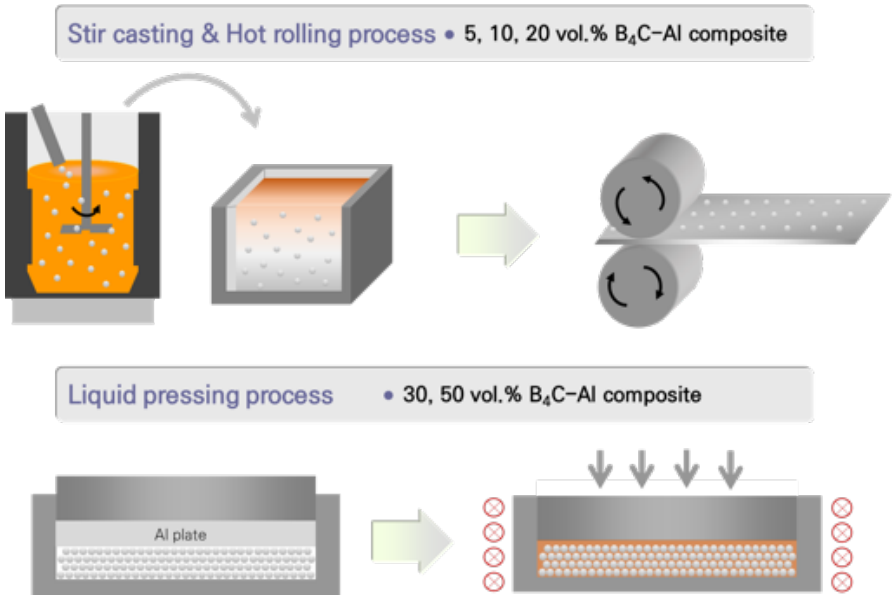

Figure 1. Schematic illustration of the B_4C–Al MMC fabrication process: (top) stir casting and hot rolling processes for low vol.% MMC samples (5, 10, and 20 vol.%) and (bottom) liquid pressing process for high vol% MMC samples (30 vol.% and 50 vol%).

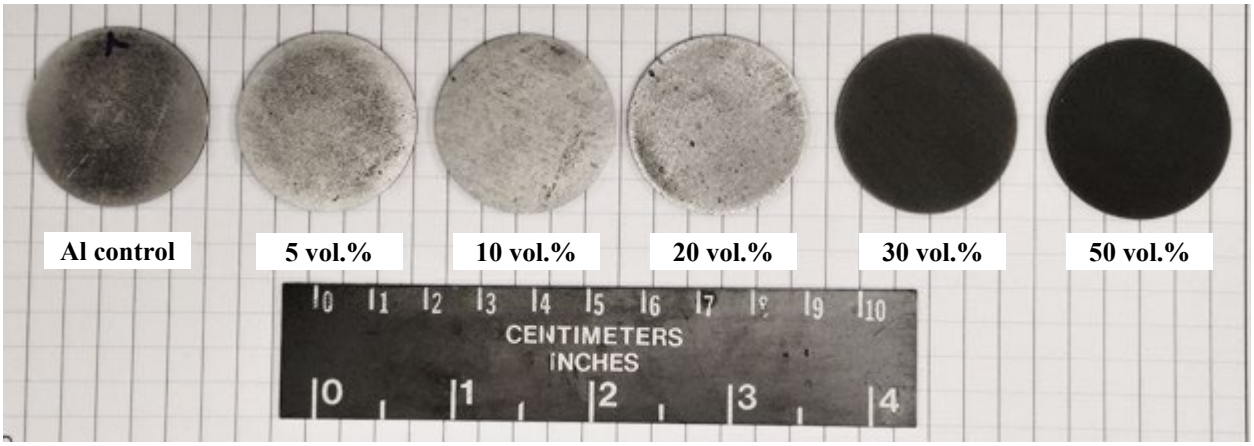

Figure 2. Image of a pristine Al6061 control and B_4C-Al MMC disk samples fabricated by the stir casting and hot rolling processes (5, 10, and 20 vol.%) and the liquid pressing process (30 vol.% and 50 vol.%).

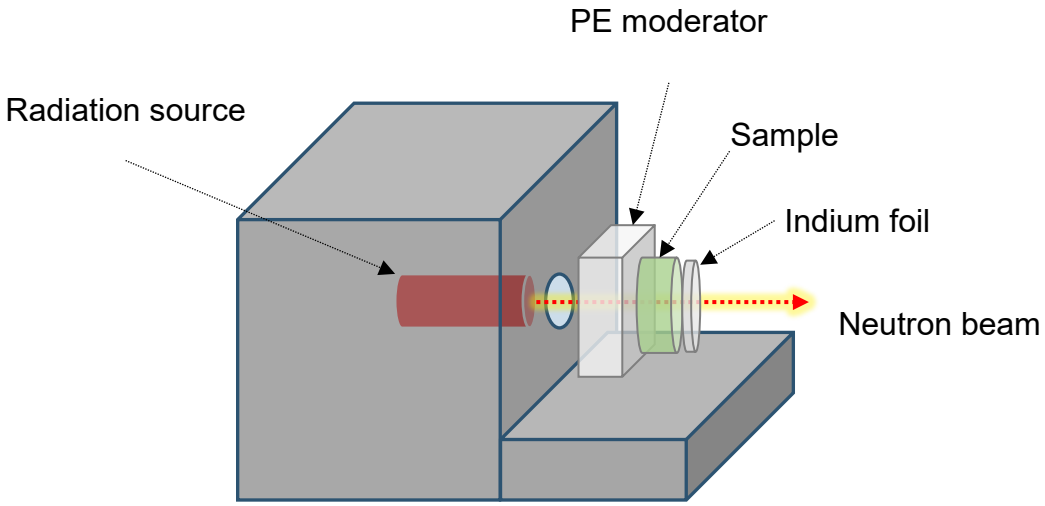

Figure 3. Setup of neutron shielding test at NASA Langley Research Center using the Am-Be neutron source, PE moderator block, and indium circular foil.

2.3. Modeling

In addition to experimental studies, we used the On-Line Tool for Assessment of Radiation in Space (OLTARIS) developed by NASA Langley Research Center (LaRC) to model B_4C-Al MMCs under various space radiation environments. The space radiation shielding effectiveness of the B_4C-Al samples were modeled for GCR and SPE radiations, using the deterministic code from NASA LaRC, HZETRN (High Z and Energy TRanNsport) based on the Boltzmann transport equation [15]. The web-based OLTARIS allowed us to utilize the most up-to-date version of HZETRN and the nuclear physics model such as NUCFRG2 (NUClear FRaGmentaion2) to improve the contributions from secondary nuclear fragmentations of nucleons and light ions [16,17]. For space radiation environments provided by OLTARIS, the Badhwar-O'Neill (BON) 2014 spectrum [18] and the August 1972 King proton spectrum [19] were selected for the GCR and SPE models, respectively, and used for free space, Lunar, and Martian surface cases.

3. Results and Discussion

B_4C-Al MMC samples with various B_4C concentrations (5, 10, 20, 30, and 50 vol.%) were examined with SEM to assess the quality of dispersion, which is shown in Figure 4. The first three samples (5, 10, and 20 vol.%) were prepared by the stir casting and hot rolling process, and the rest (30 vol.% and 50 vol.%) were prepared by the liquid pressing process. The B_4C inclusions were uniformly distributed without any noticeable agglomerates for all samples. The samples prepared by the stir casting and hot rolling process appear slightly aligned along the hot rolling direction (Figures 4a-c). The stir cast samples before hot rolling showed homogeneous dispersion without preferred alignment [14, Figures 1a-c therein].

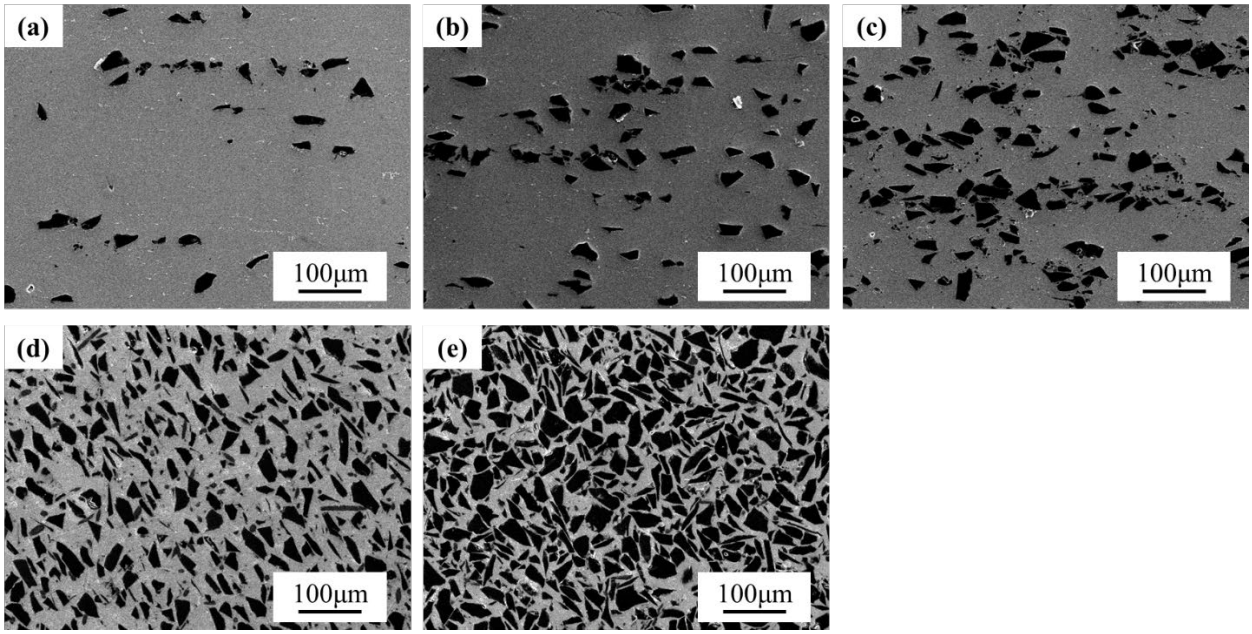

Figure 4. SEM micrographs of B_4C–Al MMC samples fabricated by the stir casting and hot rolling processes for (a) 5 vol.%, (b) 10 vol.%, and (c) 20 vol.%, and the liquid pressing method for (d) 30 vol.%, and (e) 50 vol.% B_4C. Individual B_4C particles are represented by dark objects in the SEM images.

The mechanical reinforcement was assessed by a tensile test at room temperature. Both tensile strength and modulus increased significantly with the B_4C inclusions compared with pristine Al6061 at all concentrations as shown in Figure 5. The tensile strength increased with increasing B_4C concentration and reached the maximum at 20 vol.% (over 50% increase), and then decreased at 30 vol.% and 50 vol.%. This attests the efficacy of B_4C as a mechanical reinforcing inclusion. The tribological study of these composites reported with the same systems [14] showed that wear volume was significantly reduced with increasing B_4C concentration up to 50 vol.%, which supports the tensile test results. Decrease in tensile strength at 30 vol.% and 50 vol.% B_4C-Al MMC samples is likely to be arisen from the different type of the process, where the liquid pressing process was employed without a hot rolling. Nevertheless, the tensile strengths of 30 vol.% and 50 vol.% MMC also exhibited greater strength than that of the pristine Al6061 control. The tensile strength at an elevated temperature (200˚C) was also measured for all of the samples, which is shown in Figure 6. The tensile strength was increased about 40% with B_4C inclusion for all concentrations at 200˚C in comparison with that of the pristine Al6061, and greater than that of pristine Al6061 measured at room temperature. Vickers hardness also increased with increasing B_4C concentration, which is shown in Table 1. The Vickers hardness (H_v) of Al6061 was 113.0 ± 7.2, which was increased about 40% up to 157.6 ± 7.7 with 20 vol.% B_4C inclusion. The uniform incorporation of B_4C inclusion increased both tensile strength, modulus, and hardness effectively, which is consistent to the improved wear resistance reported earlier [14].

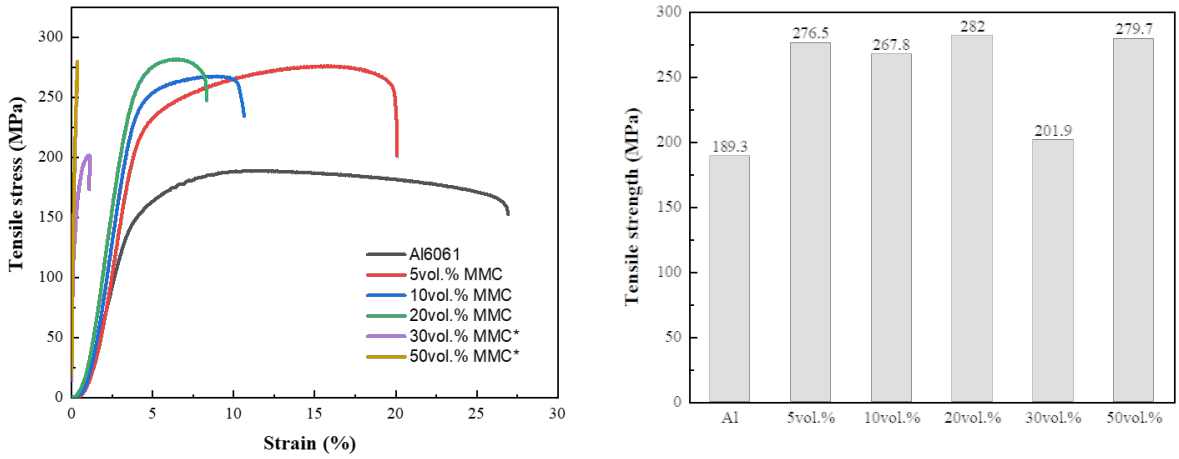

Figure 5. Tensile test result of Al6061 and B_4C–Al6061 MMC samples at a room temperature.

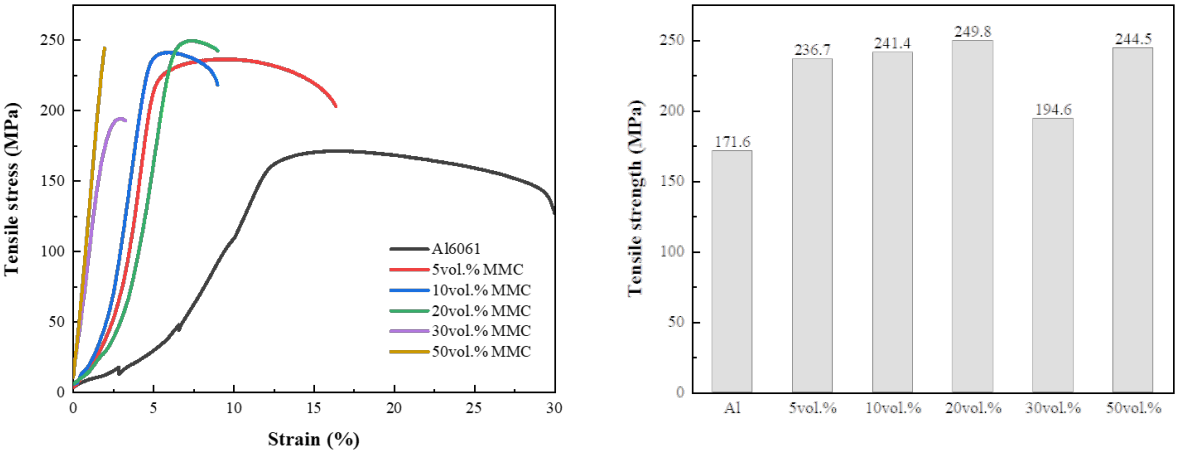

Figure 6. Tensile test result of Al6061 and B_4C–Al6061 MMC samples at an elevated temperature (200˚C).

Table 1. Vickers hardness (H_v) of Al6061 and B_4C-Al6061 MMCs.

Sample	Al6061	5%B_4C/Al6061	10%B_4C/Al6061	20%B_4C/Al6061
Hardness (H_v)	113.0 ± 7.2	120.2 ± 6.5	127.4 ± 5.2	157.6 ± 7.7

The effects of B_4C concentration on the thermal conductivity of the MMC samples were investigated at both room temperature and an elevated temperature (200˚C). Thermal conductivity of B_4C is around 20 W/mK to 40 W/mK [20] while the measured thermal conductivity of the pristine Al6061 at room temperature is about 156 W/mK. The thermal conductivity of the B_4C-Al6061 MMC samples decreased gradually with increasing B_4C concentration at both room temperature and 200 ˚C, as shown in Figure 7, which also indicates a uniform dispersion of B_4C particles in Al6061 matrix. The thermal conductivity of the MMC samples measured at an elevated temperature (200˚C) increased overall when compared with those at room temperature as expected for metals, as shown in Figure 7. This increase demonstrates that B_4C inclusion can control not only mechanical properties, but also thermal properties very effectively.

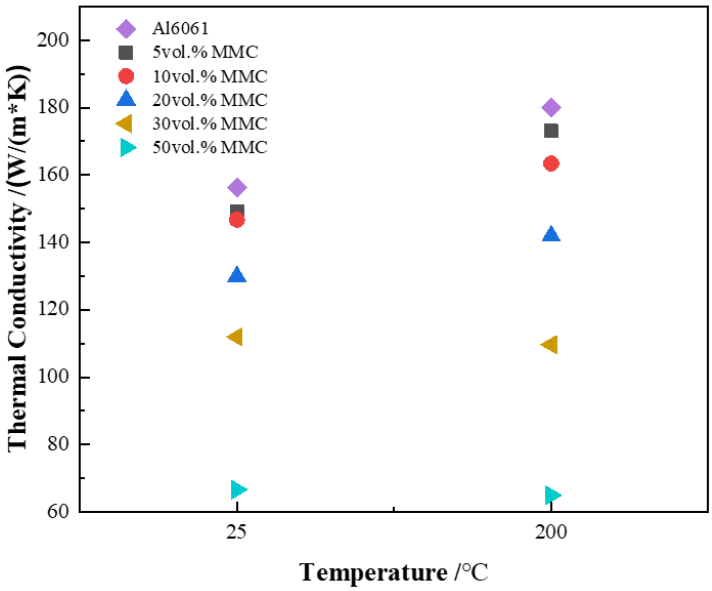

Figure 7. Thermal conductivity of the Al6061 control and B_4C- Al6061 MMC samples.

The neutron shielding test was conducted for the Al6061 control and B_4C-Al6061 MMC samples via the ^{115}In foil activation. The stable isotope of ^{115}In was exposed to neutron radiation and activated to ^{116}In along with the release of a gamma (γ) particle, and the reaction of interest can be expressed in a shorthand notation.

$$^{115}In(n,\gamma)^{116}In$$

The radioactive decay spectra of the fully activated indium foils with and without shielding materials after overnight exposure from the neutron source are shown in Figure 8. The activation at saturation or the Geiger-Mueller (GM) probe count at time t = 0 was determined for each shielding sample by extrapolation of the count plot to t = 0, and the results are summarized in Table 1 along with shielding thickness (or areal density), shielding percentage, and mass absorption coefficient. The shield thickness (g/cm^2) was obtained by multiplying the measured thickness in cm by the material density in g/cm^3. The shielding percentage or percent of radiation shielded by the sample was determined by the following equation.

$$\%\ shielded = 100 - (A/A_0 \times 100)$$

where A_o, is the average initial activity of unshielded In foil, and A, the average initial activity of shielded foil. To normalize the shielding effectiveness with different thickness and density of each sample, the normalized neutron shielding effectiveness was determined by mass absorption cross-section (or coefficient, μ_m) of the material, which can be calculated using the following equation:

$$\mu_m = -\frac{1}{d \cdot t}\ln\left(\frac{A}{A_0}\right)$$

where t is the sample thickness and d is the sample density.

As shown in Figure 8, the decay curve of the pure Al6061 sample (gray solid circle) showed a similar curve to that of the bare foil (sky blue solid circle) without shielding material, which indicates very low shielding effectiveness of the pristine Al6061 (1.1% shielding). On the other hand, the B_4C-Al MMCs exhibited excellent shielding effectiveness (29.9% shielding) even

with 5 vol.% B_4C. With increasing B_4C volume fraction, shielding effectiveness increased significantly and reached 75.5% shielding at 50 vol.% even with less than 0.5 g/cm^2 shielding thickness (areal density). The normalized neutron mass absorption coefficients with different thickness and density of each sample are shown in Table 1. By adding 5 vol.% B_4C, the shielding effectiveness improved 24 times greater than the pristine aluminum alloy and gradually increased up to 115 times at 50 vol.% with the same areal density. Since the neutron shielding effectiveness of the pristine Al6061 is negligible and the neutron capture cross-section of carbon is also negligible (~1 x 10^{-5} barns), the outstanding shielding effectiveness is arisen from the presence of boron in B_4C because of the high neutron capture cross-section (~760 barns for natural boron) and their excellent dispersion without aggregates throughout the MMC.

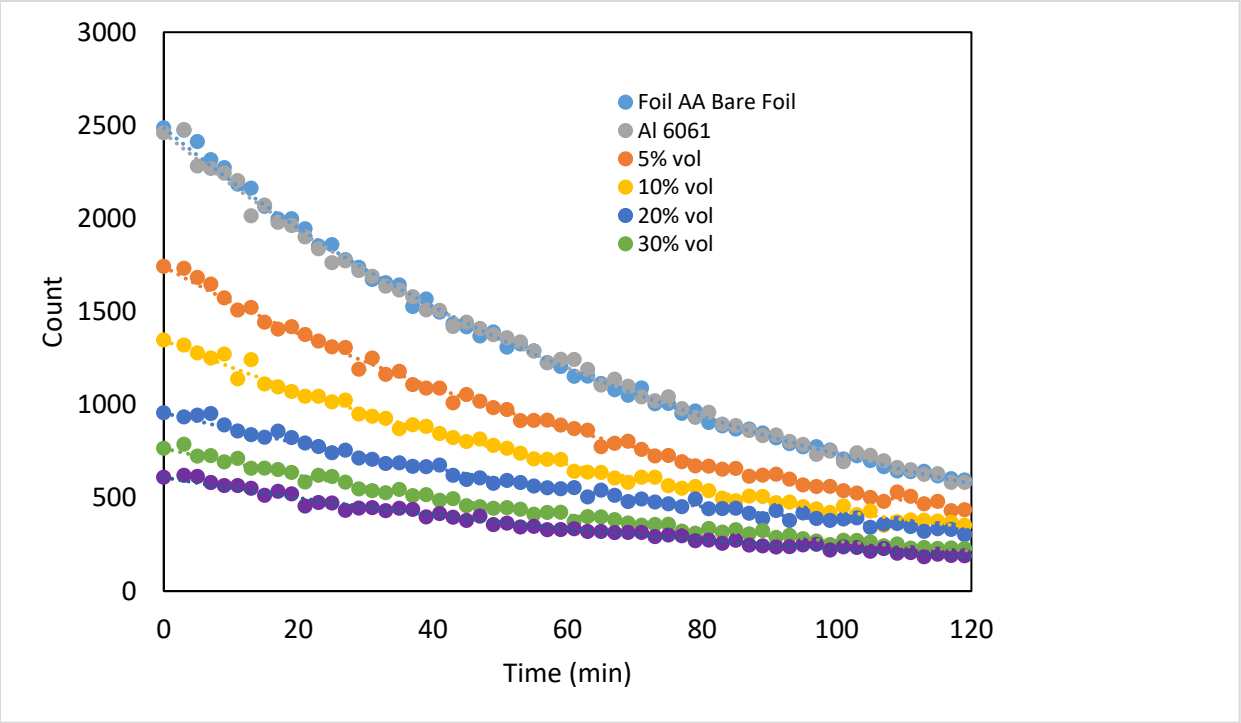

Figure 8. Radiation counts of indium foil sample with and without shielding materials B_4C-Al6061 MMC samples.

Table 2. Summary of radioactive measurement recorded by GM probe, areal density, % shielding, and mass absorption coefficient of B_4C-Al6061 MMC samples.

Description	Average A_0	Trial 1 A	Trial 2 A	Average A	Areal Density (g/cm2)	Linear Absorption (cm-1)	Linear Absorption (mm-1)	% shielded
Bare Foil (AA)	2486.2	-	-	-	-	-	-	-
Al 6061	-	2455.8	2462.5	2459.2	0.4256	0.07	0.01	1.1
B4C 5 % vol	-	1788.0	1696.1	1742.1	0.4741	2.01	0.20	29.9
B4C 10% vol	-	1384.3	1309.8	1347.1	0.4750	3.42	0.34	45.8
B4C 20% vol	-	947.8	964.6	956.2	0.4773	5.18	0.52	61.5
B4C 30% vol	-	755.1	776.5	765.8	0.4300	6.94	0.69	69.2
B4C 50% vol	-	600.1	620.3	610.2	0.4269	8.18	0.82	75.5

To understand the shielding effectiveness of B_4C-Al MMC against GCR and SPE radiations in space, the OLTARIS (On-Line Tool for Assessment of Radiation in Space) computational code was used to simulate space radiation environment. The dose equivalent was calculated for a human within a space vehicle made of a series of B_4C/Al6061 MMCs along with pure boron, polyethylene, and magnesium borohydride ($Mg(BH_4)_2$, MBH in short) for comparison. The dose equivalent spectra computed for free space GCR and SPE environment are shown in Figures 9 and 10, respectively. The results of these studies for the series of materials indicate that polyethylene $(C_2H_2)_n$ and MBH showed the best shielding effectiveness for both GCR and SPE throughout the entire areal density because of high hydrogen content of the materials. The GCR particles, the most challenging to shield, are primarily positively charged and interact with materials mainly by Coulomb interactions with the negative electrons and positive nuclei in the materials and, to a much smaller extent, by collisions with atomic nuclei in the materials. For these reasons, the energy loss of GCR particles increases approximately with the charge-to-mass ratio of the materials. Hydrogen (H), with the highest charge-to-mass ratio of any element, provides the best shielding [21]. In addition, hydrogen is very effective against GCR and SPE radiation because it does not generate a cascade of secondary radiation source unlike high atomic number (Z) elements. On the other hand, boron especially ^{10}B isotope possesses one of the largest neutron absorption cross-sections among low Z materials, which can shield neutron very effectively while producing less secondary radiation source from GCR and SPE radiation than metal alloys such as aluminum alloys. Therefore, MBH can be the best shielding material against all GCR, SPE, and neutron radiations with high hydrogen content (14.93%, greater than that of PE, 14.37%) and high boron content (40.08%) [22].

It is interesting to note that the dose equivalent initially decreases until approximately 50 g/cm^2 areal density and increases up to around 200 g/cm^2 to reach a maximum, and then decreases gradually with increasing shielding thickness for the pristine Al6061 as seen in Figure 9. The increase in dose equivalent is likely to be arisen from the buildup of mainly neutrons along with minor contributions from pions, muons, electrons, positrons, and photons produced by secondary radiations when the GCR goes through the Al6061 [23]. The same trend is shown under the free space SPE environment (Figure 10). The adverse effect by the secondary radiations were suppressed by incorporating B_4C inclusions in the Al6061 as seen in Figures 9 and 10 because the incorporation of greater charge-to-mass ratio B_4C and the presence of boron with high neutron absorption cross-section can minimize generation of secondary neutrons in the Al6061 matrix. With 50 vol.% B_4C, the dose equivalent of the B_4C-Al MMC drops almost a half of that of the pristine Al6061 without B_4C. The dose equivalent can be further suppressed if ^{10}B-enriched B_4C is used instead of naturally occurring B_4C because of the greater neutron absorption cross-section of ^{10}B (3840 barns, at 300 K) as shown in Figure 11. Consequently, the boron-containing inclusions such as B_4C can serve as an excellent shielding material against GCR and SPE as well as neutron radiation in space environment. On lunar and Mars surfaces, shielding effectiveness of B_4C can be more pronounced where more albedo neutron radiation is produced from the regolith surfaces (Figure 12). Earth and Mars's orbits meet an ideal alignment at closest distance every 26 months, which would be generally the best time for the most energy-efficient trip to Mars. Assuming the outgoing trip to Mars would take nine months, the surface exploration, three months, and the returning trip to Earth, nine months, the total round-trip to Mars would take 21 months. Using the average areal density of space flight vehicle materials (25 g/cm^2) and the theorized duration of a Mars mission (21 months), the total combined dose equivalent of the 21-month Mars mission was estimated for each material at 25 g/cm^2 shielding thickness, which is shown in Figure 13. For comparison, the red and green lines indicate lifetime career effective dose limits 1000 mSv and 600 mSv for 25-year-old female astronaut and recently recommended universal limit independent of age and gender, respectively [24]. The total dose equivalent for a roundtrip mission with 25 g/cm^2 pristine Al6061 vehicle is beyond the lifetime career limit or 1000 mSv. The total dose equivalent significantly lessens for vehicles with higher boron and hydrogen content materials. By incorporating 60 vol.% B_4C in Al6061, the total dose equivalent

falls below the 1000 mSv astronaut lifetime limit, which makes the round-trip Mars mission safer for astronauts, but still above the new limit or 600 mSv. To limit the total radiation exposure below 600 mSv, high hydrogen and boron containing shielding materials such as MBH and PE should be employed or thicker shielding is required to protect astronauts.

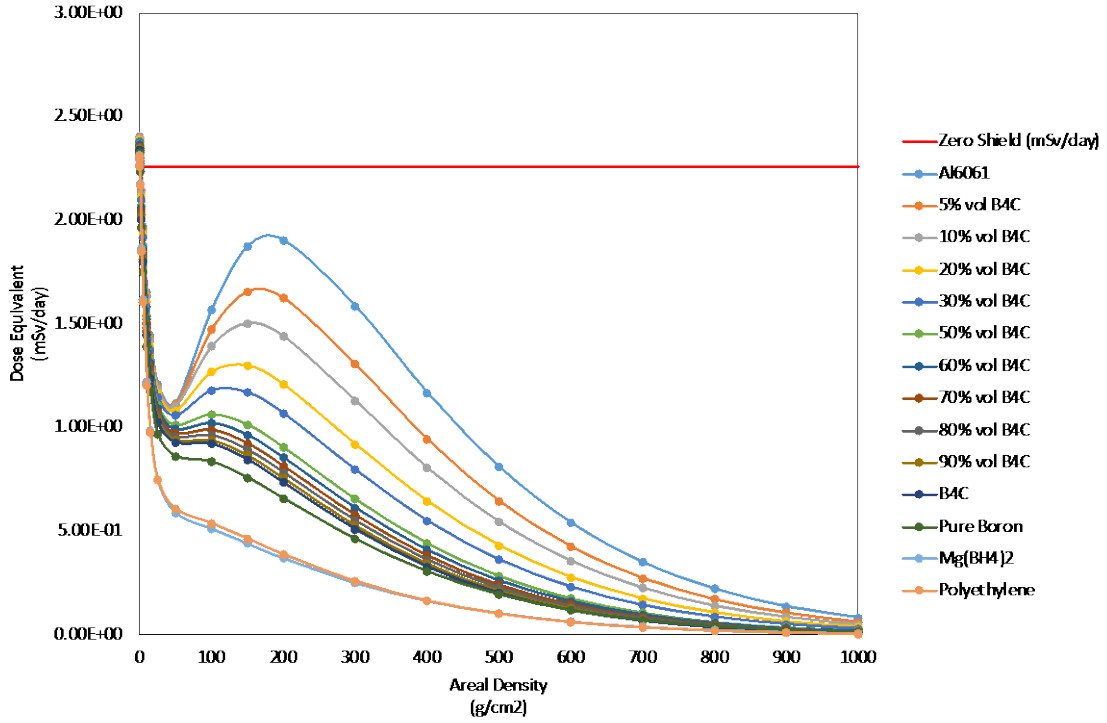

(a)

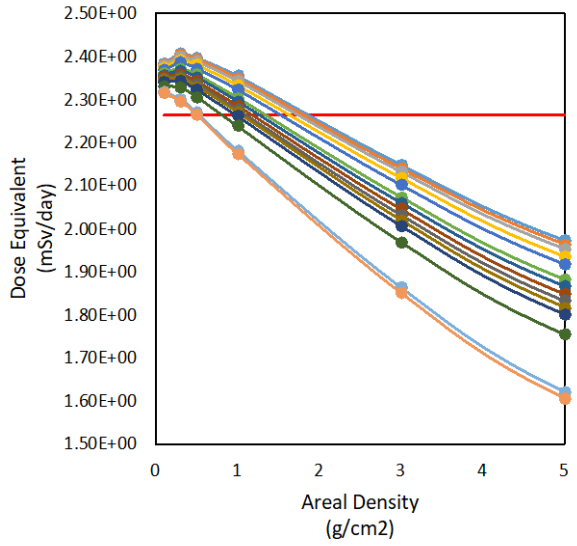

(b)

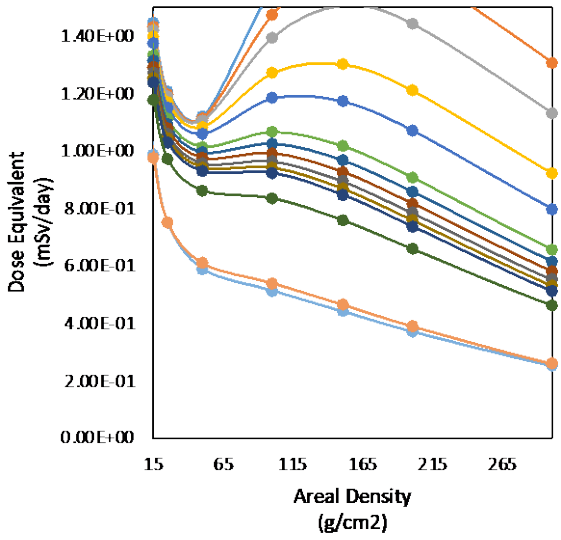

(c)

Figures 9. (a) The dose equivalent of the materials in a Free Space GCR environment; (b) the initial negative effect often found in smaller areal densities; (c) the suppression of the secondary neutrons by increasing boron and hydrogen content.

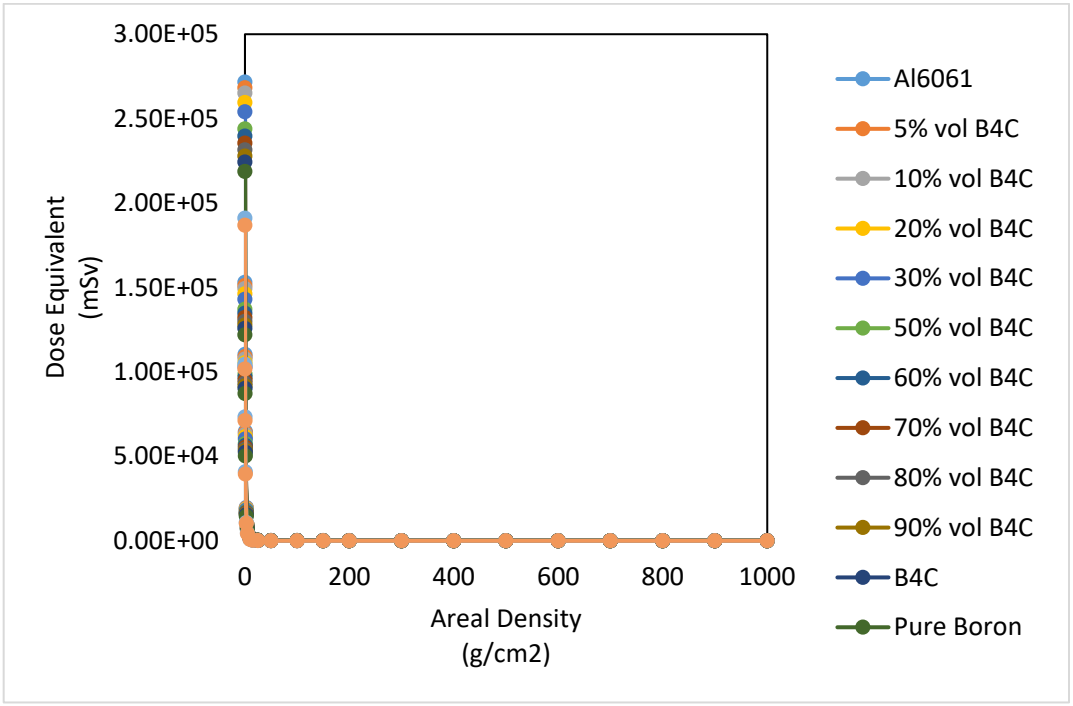

(a)

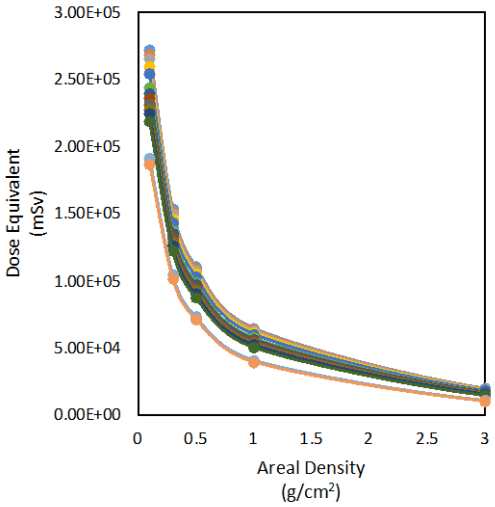

(b)

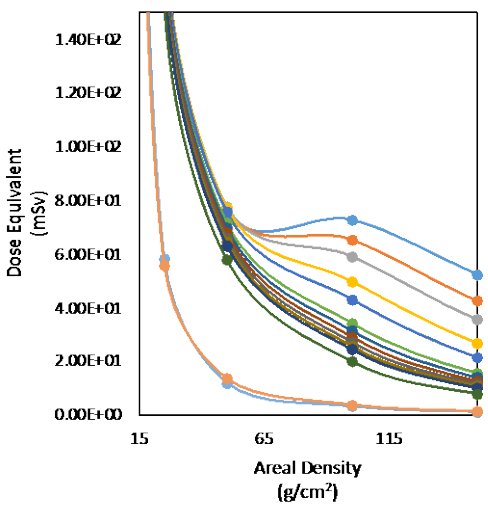

(c)

Figure 10. (a) The dose equivalent of the materials in the Free Space SPE environment; (b) the initial shielding for low areal densities; (c) the suppression of the secondary neutrons by increasing boron and hydrogen content.

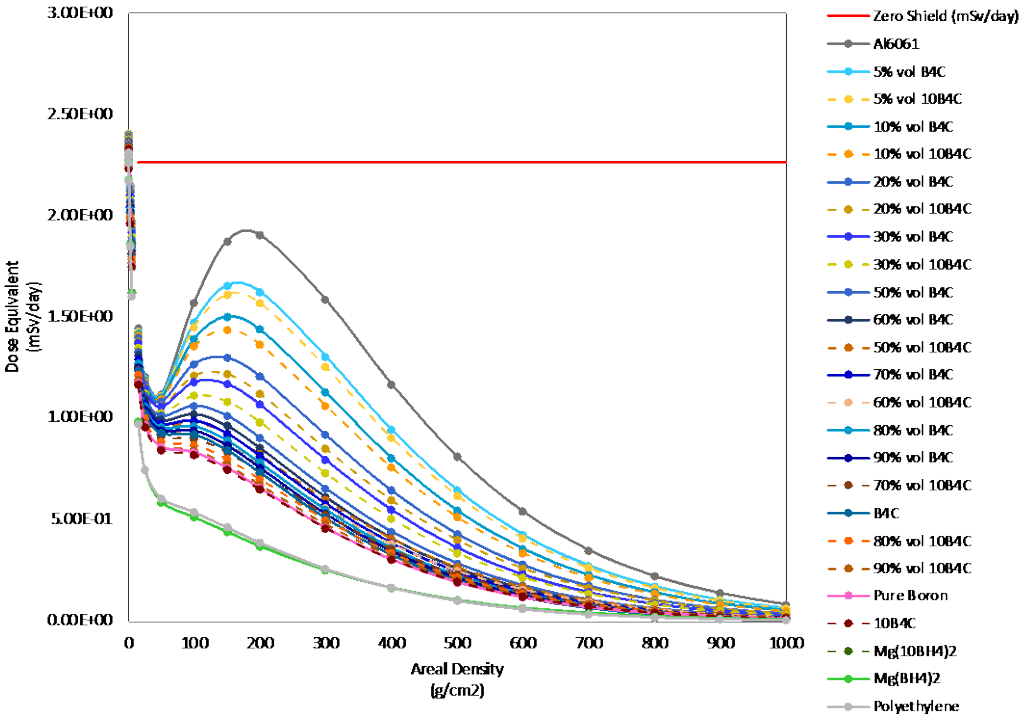

Figure 11. The dose equivalent of the materials including ^{10}B enriched B_4C/Al6061 in a Free Space GCR environment.

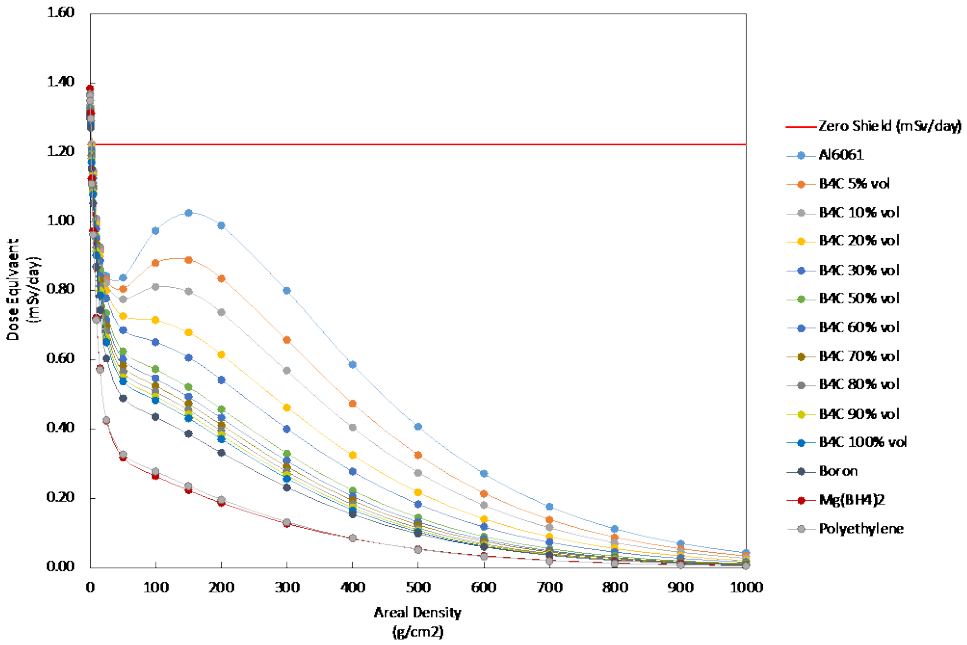

(a)

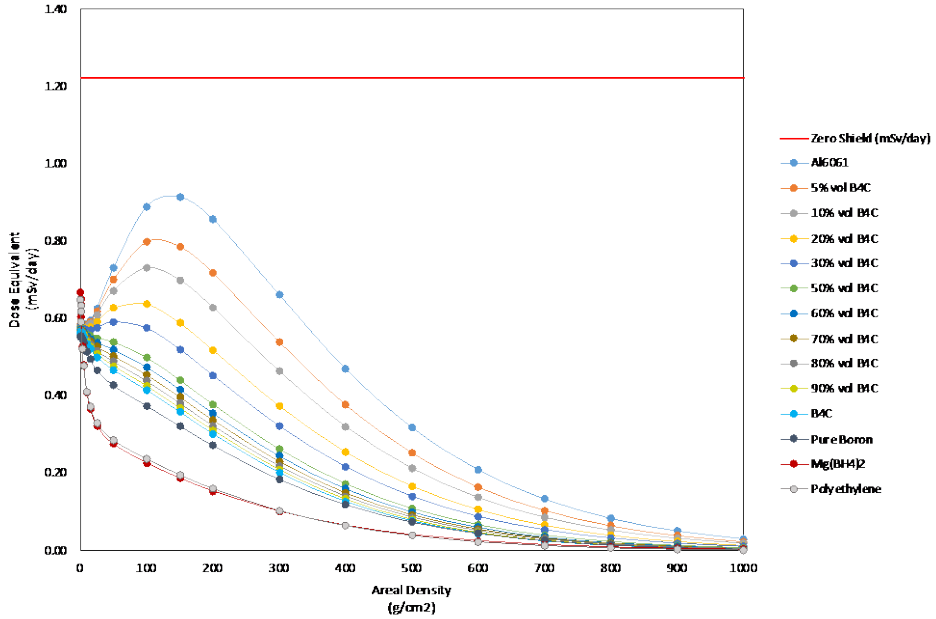

(b)

Figures 12. The dose equivalent of the materials on (a) Lunar surface/GCR environment and (b) Mars surface/GCR environment.

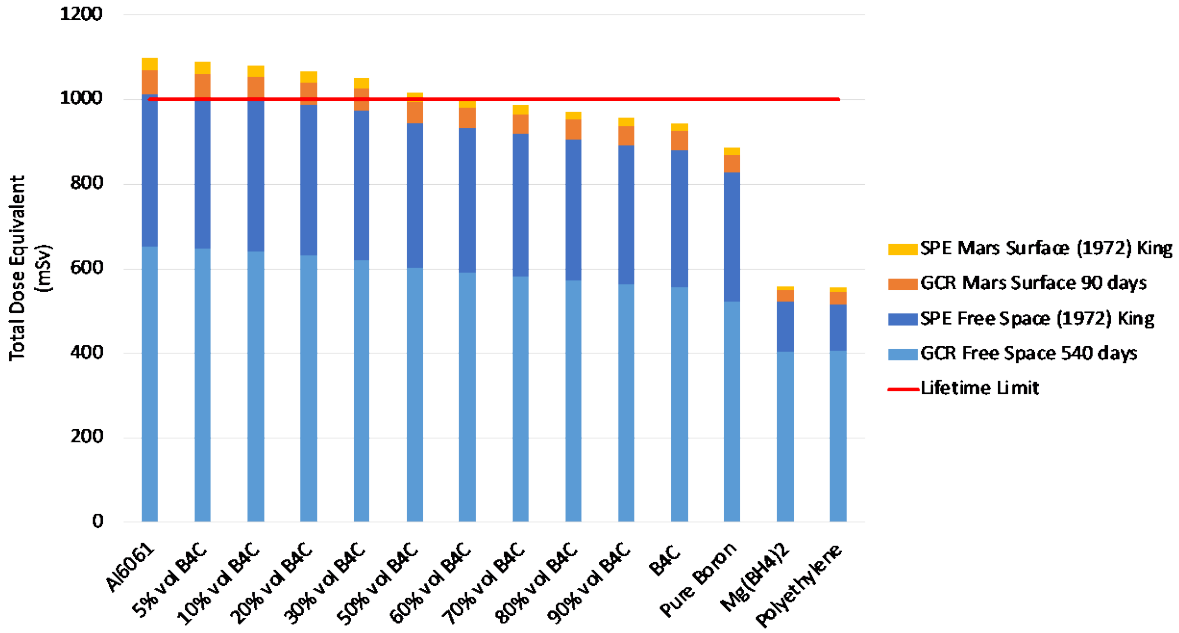

Figure 13. The total dose equivalent for a roundtrip mission using the average areal density of various space flight materials and the theorized duration of a Mars mission. The total dose equivalent for a roundtrip mission is significantly lower for vehicles with higher boron and hydrogen content materials. From 60 vol.% B_4C and on the total dose equivalent falls below the 1000 mSv astronaut lifetime limit established by Johnson Space Center. This decrease in dose equivalent could increase a mission period by up to 409 more days leading to the execution of vital research.

4. Conclusion

The boron-containing B_4C reinforcement was successfully incorporated into Al6061 matrix using both stir casting/hot rolling and liquid press processing techniques. Test results revealed that both mechanical and thermal properties can be controlled effectively with B_4C inclusions. Tensile strength and modulus as well as hardness increased with increasing B_4C composition, which is consistent with the wear resistance improvement reported elsewhere [14]. Furthermore, adding B_4C inclusions offered excellent radiation shielding capabilities against all of neutron, GCR, and SPE space radiations. Combining mechanical robustness, wear resistance, and radiation shielding potential, B_4C-Al6061 MMCs can be a great resource applicable for a sustainable space exploration on dusty Lunar and Mars surfaces with much reduced maintenance and repair needs. Further refinement of this composite material would greatly elevate and warrant the safe and productive future human space exploration missions including the Artemis program.

5. References

1. NASA's Lunar Exploration Program Overview. NASA, September 2020. https://www.nasa.gov/sites/default/files/atoms/files/artemis_plan-20200921.pdf.
2. Smith, M., Craig, D., Herrmann, N., Mahoney, E., Krezel, J., McIntyre, N., and Goodliff, K., "The Artemis Program: An Overview of NASA's Activities to Return Humans to the Moon," IEEE Aerospace Conference, (2020): 1-10.

3. Daines, Gary, “Commercial Lunar Payload Services,” NASA, March 14, 2019, https://www.nasa.gov/content/commercial-lunar-payload-services.
4. Edmonds, L. D., Barnes, C. E., and Scheick, L. Z., “An Introduction to Space Radiation Effects on Microelectronics,” Jet Propulsion Laboratory, NASA, JPL Publication 00-06, 2000.
5. Zheng, Y., Ganushkina, N., Jiggens, P., Jun, I., Meier, M., Minow, J., O'Brien, T. P., Pitchford, D., Shprits, Y., Tobiska, W. K., Xapsos, M., Guild, T., Mazur, J., Kuznetsova, M., “Space Radiation and Plasma Effects on Satellites and Aviation: Quantities and Metrics for Tracking Performance of Space Weather Environment Models,” Space Weather 17, (2019): 1384-1403.
6. Miroshnichenko, Leonty, *Radiation Hazard in Space*, Vol. 297. Springer Science & Business Media, 2003.
7. Chin, G., Scott, B., Foote, M., James, G., Justin, K., Keller, J., Litvak, M., Mitrofanov, I., Paige, D., Raney, K., Robinson, M., Sanin, A., Smith, D., Spence, H., Spudis, P., Stern, S. A., and Zuber, M., “Lunar Reconnaissance Orbiter Overview: The Instrument Suite and Mission,” Space Science Reviews 129, (2007): 391-419.
8. Clowdsley, M. S., Wilson, J. W., Kim, M.-H. Y., Singleterry, R. C., Tripathi, R. K., Heinbockel, J. H., Badavi, F. F., and Shinn. J. L., “Neutron Environments on the Martian Surface,” Physica Medica 17, (2001): 94-96.
9. Wilson, J. W., Clowdsley, M. S., Shinn, J. L., Singleterry, R. C., Tripathi, R. K., Cucinotta, F. A., Heinbockel, J. H., Badavi, F. F., and Atwell, W., “Neutrons in Space: Shield Models and Design,” Issues. No. 2000-01-2414. SAE Technical Paper, 2000.
10. Getselev, I., Rumin, S., Sobolevsky, N., Ufimtsev, M., and Podzolko, M., “Absorbed Dose of Secondary Neutrons from Galactic Cosmic Rays Inside the International Space Station,” Advances in Space Research 34, (2004): 1429-1432.
11. Köhler, J., Zeitlin, C., Ehresmann, B., Wimmer-Schweingruber, R., Hassler, D., Reitz, G., Brinza, D., Weigle, G., Appel, S., Bottcher, S., Bohm, E., Burmeister, S., Guo, J., Martin, C., Posner, A., Rafkin, S., Kortmann, O., “Measurements of the Neutron Spectrum on the Martian Surface with MSL/RAD,” Journal of Geophysical Research: Planets 119, (2014): 594-603.
12. Kim, M.-H. Y., Wilson, J. W., Thibeault, S. A., Nealy, J. E., Badavi, F. F., and Kiefer, R. L., “Performance Study of Galactic Cosmic Ray Shield Materials,” NASA-TP-3473, NASA, 1994.
13. Carron, Neal Jay, “An Introduction to the Passage of Energetic Particles Through Matter,” CRC Press, 2006.
14. Lee, D., Kim, J. Lee, S.-K., Kim, Y., Lee, S.g-B., and Cho, S., “Effect of Boron Carbide Addition on Wear Resistance of Aluminum Matrix Composites Fabricated by Stir Casting and Hot Rolling Processes,” Metals 11, (2021): 989.
15. Wilson, J. W., Shinn, J. L., Tripathi, R. K., Singleterry, R. C., Clowdsley, M. S., Thibeault, S. A., Cheatwood, F. M., Schimmerling, W., Cucinotta, F. A., Badhwar, G. D., Noor, A. K., Kim, M.-H. Y., Badavi, F. F., Heinbockel, J. H., Miller, J., Zeitlin, C., Heilbronn L., “Issues in Deep Space Radiation Protection,” Acta Astronautica 49, (2001): 289-312.
16. Singleterry, R. C., Blattnig, S. R., Clowdsley, M. S., Qualls, G. D., Sandridge, C. A., Simonsen, L. C., Slaba, T. C., Walker, S. A., Badavi, F. F., Spangler, J. L., Aumann, A. R., Zapp, E. N., Rutledge, R. D., Lee, K. T., “OLTARIS: On-Line Tool for the Assessment of Radiation in Space,” Acta Astronautica 68, (2011): 1086-1097.
17. Norbury, J. W., Slaba, T. C., Aghara, S., Badavi, F. F., Blattnig, S. R., Clowdsley, M. S., Heilbronn, L. H., Lee, K., Maung, K. M., Mertens, C. J., Miller, J., Norman, R. B., Sandridge, C. A., Singleterry R., Sobolevsky, N., Spangler, J. L., Townsend, L. W., Wernerth, C. M., Whitman, K., Wilson, J., Xu, S. X., Zeitlin, C., “Advances in Space Radiation Physics and Transport at NASA,” Life Sciences in Space Research 22, (2019): 98-124.

18. O'Neill, Patrick M, “Badhwar–O'Neill 2010 galactic cosmic ray flux model—Revised,” IEEE Transactions on Nuclear Science 57, (2010): 3148-3153.
19. King, Joseph H., "Solar Proton Fluences for 1977-1983 Space Missions," Journal of Spacecraft and Rockets 11, (1974): 401-408.
20. https://www.azom.com/properties.aspx?ArticleID=75
21. Thibeault, S. A., Kang, J. H., Sauti, G., Park, C., Fay, C. C. and King, G. C. “Nanomaterials for Radiation Shielding,” MRS Bulletin 40, (2015): 836-841.
22. “Evaluating the Effectiveness of Common Aerospace Materials at Lowering the Whole Body Effective Dose Equivalent in Deep Space,” NASA-TP, *in preparation*.
23. Norbury, J. W., and Slaba, T. C., “Space Radiation Accelerator Experiments – The Role of Neutrons and Light Pions,” Life Sciences in Space Research 3, (2014): 90-94.
24. Cucinotta, F. A., Schimmerling, W., Blakely, E. A., and Hei, T. K., “A Proposed Change to Astronaut Exposures Limits is a Giant Leap Backwards for Radiation Protection,” Life Sciences in Space Research 31, (2021): 59-70.